Article

A Label-Free and Regenerable Aptasensor for Real-Time Detection of Cadmium (II) by Dual Polarization Interferometry

Yu Xue, Yu Wang, Shuang Wang, Mengxia Yan, Jianshe Huang, and Xiurong Yang

Anal. Chem., **Just Accepted Manuscript** • DOI: 10.1021/acs.analchem.0c01710 • Publication Date (Web): 03 Jul 2020

A Label-Free and Regenerable Aptasensor for Real-Time Detection of Cadmium (II) by Dual Polarization Interferometry

Yu Xue,[†,‡] Yu Wang,[†,‡] Shuang Wang,[†,‡] Mengxia Yan,[†,‡] Jianshe Huang,*[,†] Xiurong Yang*[,†,‡]

† State Key Laboratory of Electroanalytical Chemistry, Changchun Institute of Applied Chemistry, Changchun, Jilin 130022, China

‡ University of Science and Technology of China, Hefei, Anhui 230026, China

* Fax: +86 431 85689278. E-mail: xryang@ciac.ac.cn, huangjs@ciac.ac.cn

ABSTRACT: Recently, numerous aptamer-based biosensors have been developed to detect heavy metal ions. Most of aptamer-based biosensors only can be used to get some quantitative information. The mechanism of the interaction between aptamer and metal ions, however, is rarely studied. In this work, a label-free and regenerable aptamer-based biosensor was constructed using dual polarization interferometry (DPI). This aptasensor was used to investigate the real-time interaction process between cadmium (II) and its aptamer. According to the information of mass, thickness and density obtained by DPI, a Cd^{2+} concentration-dependent interaction mechanism and conformation of aptamer was proposed. At low Cd^{2+} concentration, Cd^{2+} mainly interacted with phosphate groups on aptamer, resulting in the stretched ssDNA and a few vertical hairpin structures. When adding the high concentration of Cd^{2+}, Cd^{2+} primarily bound with bases of DNA by coordination interaction and the conformation of aptamer transferred to a tight and short hairpin structure. In addition, the association rate constant (k_a), dissociation rate constant (k_d) and disassociation constant (K_D) between Cd^{2+} and its aptamer were calculated to be 96 $M^{-1} \cdot S^{-1}$, 2.11×10^{-5} S^{-1}, and 220 nM, respectively. The proposed aptasensor showed high sensitivity for Cd^{2+} detection with the detection limit of 0.61 μg/L, which was far below the 5.0 μg/L ranked by US Environmental Protection Agency. The biosensor also exhibited excellent regenerability and could be used for three cycles without obvious change in response signal. Therefore, the developed method could not only provide quantitative information, but also offered the information of conformation and kinetics for molecular interaction. This method can facilely extend to study the interaction of DNA with other ions, small molecules, or biomacromolecules.

Cadmium ion (Cd^{2+}) is considered as one of the highly toxic heavy metal ions due to its serious damages on human health and the environment.[1] Because of its wide range applications in human life such as fertilizers, fuels, plastics, toys, and several industrial products,[2, 3] and the fact that the body is short of an efficient detoxification pathway for heavy metal ions. Cd^{2+} tends to easily accumulate in many organs and tissues of humans.[4] Consequently, Cd^{2+} causes a number of diseases such as renal dysfunction, Itai-itai disease, hypertension, Alzheimer's disease (AD), and cancer.[5] The International Agency for Research on Cancer (IARC) has ranked cadmium and cadmium compounds as category I carcinogens. In order to protect humans health, the U.S. Environmental Protection Agency (EPA) limited that the maximum pollutant concentration for Cd is 5.0 μg/L in drinking water.[6] Therefore, it is necessary to monitor and detect Cd in drinking water or other environmental samples.

Aptamers, a type of artificial oligonucleotide probes, are generated by an in vitro technique termed SELEX (systematic evolution of ligands by exponential enrichment).[7, 8] Owing to the unique secondary structures, high affinity and selectivity to targets, aptamers are widely used for constructing biosensor to detect a broad range of targets, such as ions,[9, 10] small molecules,[11, 12] proteins,[13, 14] heavy metal ions[15, 16] and so on. Pei and Zhou have designed different Cd^{2+}-specific aptamers,[17, 18] based on which a number of aptamer-based biosensors have been proposed for specific recognition and detection of Cd^{2+}.[19-22] However, most of sensing platforms merely provided a simple response function and needed complicated modification process,[23-26] which seriously restricted the application of these methods. Moreover, these studies could not provide kinetics information and the real-time conformation changes of DNA aptamer on the interaction with Cd^{2+}.

Dual polarization interferometry (DPI), an evanescent optical biosensing platform, is a sensitive and effective analytical technique which can not only offer the quantitative information, but also give the real-time kinetic conformation information that related to the biomolecule interactions.[27] DPI with a long waveguide chip makes the measurements more stable and accurate than surface plasmon resonance (SPR).[28, 29] Compared with quartz crystal microbalance with dissipation (QCM-D) which only offers the estimated mass, density, or thickness of a thin film separately, DPI permits the distinct determination of change in mass, thickness, and refractive index (RI) simultaneously at the solid-liquid interface by utilizing both transverse magnetic (TM) and transverse electric (TE) polarization. Additionally, compared with other usual structure-measured technologies such as nuclear magnetic resonance (NMR), X-ray crystallography, and high-resolution mass spectrometry (HRMS),[30,31] the real time structure information can be gained from DPI technique. On the basis of above advantages, DPI have been widely applied in researching the connection between structure and function, such as studying the protein binding events which associated with Alzheimer's

disease (AD),[32] probing the interaction of DNA with small molecules,[33, 34] and metal ions,[35-37] investigating the bio-membrane reactions[38, 39] and the immobilization of polymer on the solid phase interface.[40, 41]

In this work, by utilizing the layer-by-layer assembly method, an aptasensor was established using DPI technique, and was applied to real-time study the interaction mechanism of Cd^{2+} and aptamer. Combined with spectroscopy characterization (UV-vis, CD, and FTIR), Cd^{2+} concentration-dependent interaction mechanism and aptamer conformation was proposed. We found that at lower Cd^{2+} concentration, the electrostatic interaction was primary, which was accompanying with the extended ssDNA structures and a few upstanding hairpin structures of aptamer. With the increase of Cd^{2+} concentration, electrostatic interaction and coordination interaction coexisted but the latter was dominated. Under this condition, the conformation of aptamer converted into a tight and short hairpin structure. The kinetic constants of the interaction between aptamer and Cd^{2+} were calculated by using mass binding curves. Meanwhile, the aptasensor also shows excellent reusability and high sensitivity for Cd^{2+} detection. A good linear in the range of 0.0036 to 7.28 mg/L and a lower limit of detection (0.61 μg/L) was obtained from mass calibration.

EXPERIMENTAL SECTION

Chemicals and Materials. Poly(ethyleneimine) solution (PEI, MW 750000) was provided from Sigma-Aldrich (St. Louis, MO). Cadmium (II) nitrate tetrahydrate [$Cd(NO_3)_2 \cdot 4H_2O$], magnesium chloride hexahydrate ($MgCl_2 \cdot 6H_2O$), nickel (II) acetate tetrahydrate [$Ni(Ac)_2 \cdot 4H_2O$], zinc sulfate heptahydrate ($ZnSO_4 \cdot 7H_2O$), lead (II) acetate trihydrate [$Pb(Ac)_2 \cdot 3H_2O$], barium acetate [$Ba(Ac)_2$], manganese (II) sulfate monohydrate ($MnSO_4 \cdot H_2O$) were purchased from Aladdin Chemistry Co. Ltd. (Shanghai, China). Potassium chloride (KCl), sodium chloride (NaCl) and calcium chloride ($CaCl_2$) were provided from Beijing Chemical Reagent Co. (Beijing, China). Tris (hydroxymethyl) aminomethane (Tris) was obtained from Sangon Biotechnology Co. Ltd. (Shanghai, China). All reagents were analytical grade and used as received. The DNA oligonucleotides were synthesized by Sangon Biotechnology Co. Ltd. (Shanghai, China), and the sequence are presented in Table S1. Before experiments, the thermal denaturation process of DNA probe was performed by heating at 95 °C for 5 min and then quickly cooling down to 4 ℃ to open the hairpin structure and form more single stand structures. Ultrapure water (Milli-Q water system) of 18.25 MΩ was used throughout. Before use, 10 mM Tris-HCl buffer solution (150 mM NaCl, pH 7.0) were filtered and degassed.

CD measurements and UV–vis absorption spectra characterization. CD spectra measurements were performed on a Jasco J-820 circular dichroism spectropolarimeter (Tokyo, Japan). The whole experiment process was under the nitrogen atmosphere and 100 nm/min was selected as the scanning rate for three parallel measurements in the range from 210 to 350 nm. The buffer solution (10 mM Tris-HCl, pH 7.0, 150 mM NaCl) was scanned as the background, which would be automatically subtracted from the following CD data. Before CD spectral measurement, 200 μL buffer solution containing 3 μM ssDNA probe (or control DNA) and 6.48 μM Cd^{2+}, or 3 μM ssDNA probe (or control DNA) and 32.4 μM Cd^{2+} reacted about 30 min at room temperature.

The UV-vis spectra were acquired on a CARY 500 UV–vis–NIR Varian spectrophotometer. With a high scanning rate, 10 mM Tris-HCl buffer solution (pH 7.0, 150 mM NaCl) was subtracted as the background in the spectrum range (from 190 to 350 nm). Then the mixed solution (100 μL) containing 2 μM ssDNA probe (or control DNA) and 20 μM Cd^{2+} were incubated for 30 min at room temperature.

Fourier Transform Infrared (FTIR) spectra characterization. Attenuated Total Reflectance-Fourier Transform Infrared spectra (ATR-FTIR) were recorded on a VERTEX 70 spectrometer (Bruker, Germany) over the spectral range 800 - 2000 cm^{-1}, the nominal resolution was 2 cm^{-1} with a minimum of 32 times scanning. The buffer solution (10 mM Tris-HCl, pH 7.0, 150 mM NaCl) was scanned as the background and its results would be automatically subtracted from the following ATR-FTIR data. Prior to ATR-FTIR record, the spectra of solution including 2.3% DNA (w/w) probe and 10 mM Cd^{2+} were incubated at room temperature for 30 min.

Dual Polarization Interferometry experiments. The construction of sensing platform and the interaction process of probe with Cd^{2+} were monitored by DPI instrument (AnaLight Bio200, Farfield) with a bare silicon oxynitride chip. Before DPI experiments, the chip needed to be cleaned by Piranha solution (H_2SO_4 : 30% H_2O_2=7:3) for 12 h. The DPI chip rinsed subsequently by sonicating in ethanol and ultrapure water for 6 min, respectively, and this process was repeated three times. A steam of nitrogen was swept to remove the water from the chip surface. Finally, the chip was loaded into DPI instrument. 10 mM Tris-HCl buffer solution (150 mM NaCl, pH=7.0) were used in the whole DPI experiments process at 20 ℃. The calibration process was the same as the previous report.[42] After calibration and the baseline reached stable, the flow rate of buffer solution was set at 50 μL/min, 1 mg/L PEI was introduced into both channels at 50 μL/min for 5 min and stopped for another 5 min. Then, both channels were rinsed by running buffer until the stable baseline was achieved. After that, 250 μL T30 (12 μM) was introduced into both channels for 5 min and incubated for 5 min, then the solution got back to the running buffer to obtain a steady baseline. Subsequently, to hybridize with T30, 7.2 μM probe or control DNA was introduced into both channels at a flow rate 50 μL/min for 5 min and incubated for 5 min. Finally, 250 μL Cd^{2+} with different concentration was introduced into both channels for 5 min. We stopped the experiment until all samples were introduced and the baseline attained a plateau. All experiment datum was converted into refractive index, thickness, mass, and density values and analyzed by AnaLight DAQ software.

Cd^{2+} detection in tapping water. In order to prove the practicability, the proposed aptasensor was used to detect Cd^{2+} in tapping water. The water sample was diluted to 1% by using running buffer, and then spiked with different concentrations of Cd^{2+}. The analytical process was the same as above procedure.

RESULTS AND DISCUSSION

Construction of biosensing surface based on layer-by-layer assembly method. It is critical to construct a sensitive biosensing platform for detecting Cd^{2+}. Our group had

Scheme 1. Whole process of biosensing interface construction and study of interaction between probe and Cd^{2+}

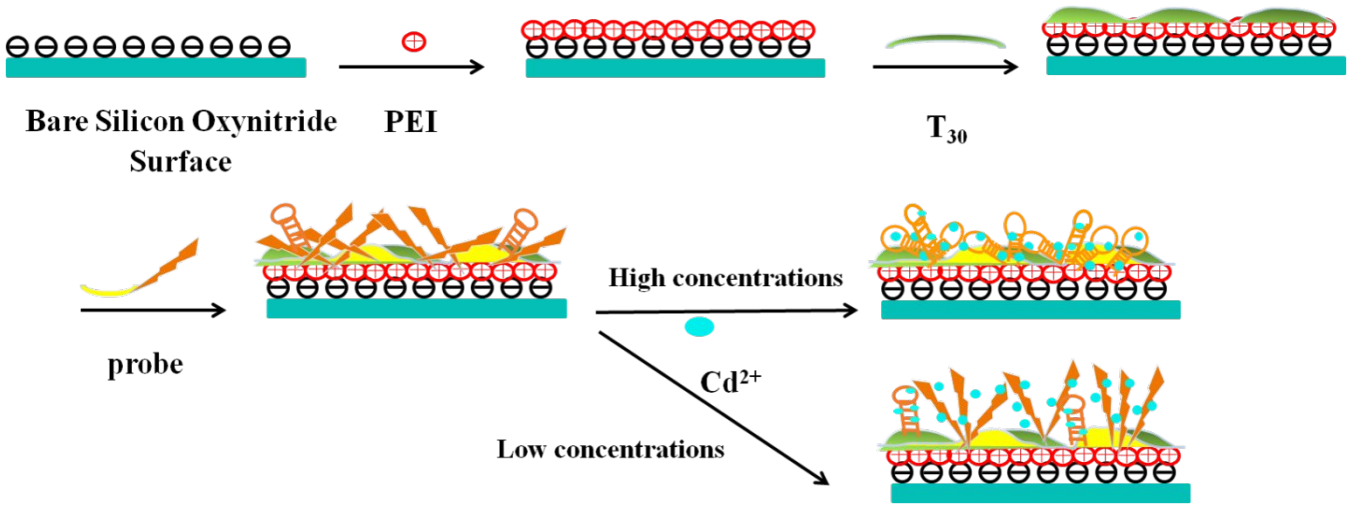

reported several methods for investigating the interaction of DNA and metal ions.[35-37] One method is to immobilize the DNA probe by electrostatic adsorption of PEI, which was simple but limited the conformational change of DNA probe on PEI layer in a way. In another method, DNA tetrahedron nanostructure was used to construct the sensing platform, which improved the flexibility and availability of DNA probe, but the preparation process is costly and complicated. Therefore, we chose a compromise layer-by-layer assembly method to prepare the sensing platform, which overcame the strong electrostatic adsorption between DNA probe and PEI, at the same time remained the flexibility of DNA probe. Scheme 1 demonstrates the layer-by-layer assembly process of biosensor interface. Cationic polymer PEI was firstly absorbed on the chip surface to reverse the charge state of chip surface. Then T30 oligonucleotides were immobilized on the chip surface through electrostatic interaction. A 40-mer DNA probe containing cadmium-specific aptamer sequence and 15-mer homoadenine sequences (A15) was intentionally designed to hybrid with T30 sequence, consequently to immobilized Cd^{2+} aptamer on the sensing platform. When Cd^{2+} was introduced into the sensing surface, the aptamer would specifically bind with Cd^{2+} and undergo conformational transition in some extents. At low Cd^{2+} concentration, electrostatic interaction between Cd^{2+} and probe made the probe more vertical. With the Cd^{2+} concentration increasing, Cd^{2+} primarily coordinated with the bases (mainly G, A and T) of probe,[18, 43] which converted the conformation of probe from flexible single strand and a few hairpins to the compact hairpin structure.

Fourier Transform Infrared (FTIR) spectroscopy study of the binding site of Cd^{2+}-aptamer. FTIR spectroscopy was firstly performed to characterize the binding site of aptamer with Cd^{2+}. According to previous literature reports,[43-45] PO_2^- stretching vibrations (symmetric and asymmetric), deoxyribose stretching of DNA backbone and ring vibrations of nitrogrnous bases (C=O, C=N stretching) were confined in the spectral region 1800-700 cm^{-1}. As shown in Figure 1, after the addition of Cd^{2+}, the peak intensity and position of probe DNA in 1800-1250 cm^{-1} were remarkably changed, the peak in this range was attributed to bases vibration.[46-49] For example, the vibrational band at 1295, 1365, 1450 and 1491 cm^{-1} disappeared and formed a new vibrational band centered at 1353 cm^{-1} which was very strong and wide. Besides, the vibrational bands at 1604, 1658 and 1708 cm^{-1} shifted to 1606, 1654 and 1704 cm^{-1}, respectively, and the intensity of them were also changed. These changes of vibrational band implied that Cd^{2+} was bound to aptamer by coordinating with bases. In the remaining region from 1250 to 900 cm^{-1}, the vibrational bands at 1016, 1089 (symmetric stretching vibration of PO_2^-), 1221 cm^{-1} (antisymmetric stretching vibration of PO_2^-), shifted to 1012, 1093, 1218 cm^{-1}, respectively, and the band at 1053 cm^{-1} disappeared, suggesting that some binding sites located in phosphate and ribose as well.[46,47,50] Therefore, it can be concluded that Cd^{2+} interacted with aptamer not only by forming coordination bonds with bases, but also through binding with phosphate. This result was consistent with the previous work.[43]

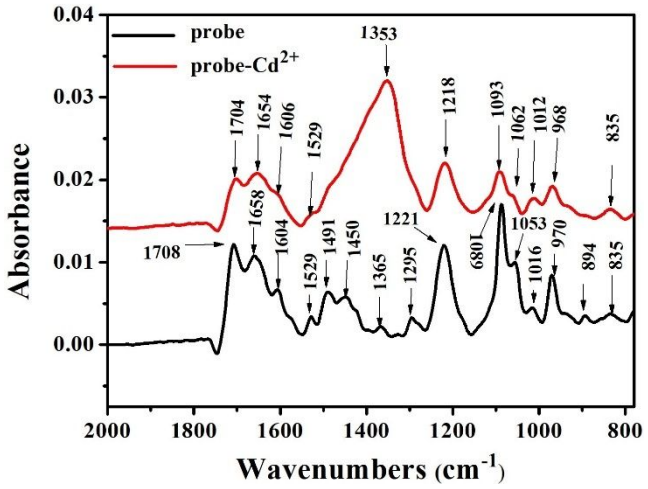

Figure 1. ATR-FTIR spectra of probe (black line) and probe-Cd^{2+} (red line) at a Cd^{2+}/DNA molar ratio 3:1 in 10 mM Tris-HCl buffer solution (pH 7.0, 150 mM NaCl).

Circular dichroism (CD) and UV-visible spectroscopic study of the interaction between Cd^{2+} and aptamer. The conformational changes of aptamer in the interaction process were verified using CD spectra. As shown in Figure 2A, there are two positive bands of probe at 218 nm and 274 nm, which was attributed to the random coil structure and the bases stacking of DNA, respectively.[51] The negative band at 247 nm was

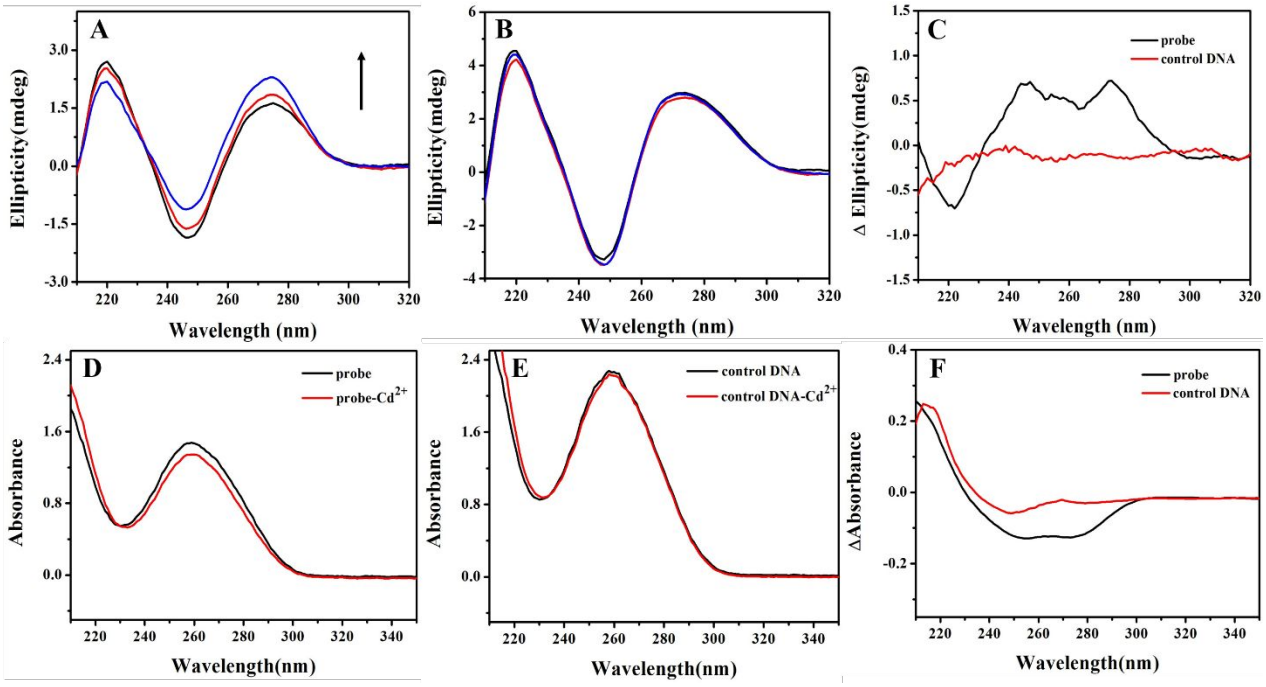

Figure 2. The CD spectra characterization of the probe (A), control DNA (B) after addition different concentrations of Cd^{2+} in 10 mM Tris-HCl buffer solution (pH 7.0, 150 mM NaCl) and their differential spectrometry (C). The UV-vis spectra characterization of the probe (D), control DNA (E) after adding different concentrations of Cd^{2+} in 10 mM Tris-HCl buffer solution (pH 7.0, 150 mM NaCl) and their differential spectrometry (F). The arrow in A shows the increase of Cd^{2+} concentration from 0 to 32.4 μM.

also observed due to the helicity of DNA.[52] With the increase concentrations of Cd^{2+}, the positive peak at 274 nm increased, while the negative peak at 247 nm and the positive peak at 218 nm decreased. However, there were negligible changes for control DNA after adding Cd^{2+} (Figure 2B). In Figure 2C, the CD differential spectrometry of the probe showed apparent doublet at 245 nm and 275 nm, but that of control DNA was approximate to a straight line. The result of CD experiment proved that Cd^{2+} bound with bases through coordination interaction, it facilitated the vertical stacking of DNA bases and changed the surface state of probe. Thus, the probe underwent a conformation change, while the change did not exist in control DNA.

After adding Cd^{2+}, the UV-vis spectra of probe DNA displayed that the intensity of absorbance peak at 260 nm decreased, while there was no obvious change in control DNA (Figure 2D-F). The absorbance of DNA at 260 nm generated from the exposed bases, and the extinction of ssDNA was higher than dsDNA.[53] Hence, the UV-vis characterization result indicated that the proportion of double-stranded structure in probe increased after interacting with Cd^{2+}. Beyond that, the temperature-dependent CD spectropolarimetry was adopted at 260 nm to further investigate the melting curves of probe with and without Cd^{2+} (Figure S1, Supporting Information). The melting temperature of the probe was determined to be about 68 ℃, corresponding to the fitting result of UNAFold software. When the Cd^{2+} was added, the melting temperature rose up to around 75 ℃, which might be ascribed to the increase of double-stranded structure promoting the melting temperature. Above characterization results suggested that the addition of Cd^{2+}coordinating with bases promoted the vertical stacking of DNA bases and increased the proportion of double strands structure in probe.

Monitoring the immobilization process of aptamer by DPI. The premise of studying the interaction between Cd^{2+} and aptamer was to successfully immobilize aptamer on the sensing surface. As displayed in Figure 3, during the real-time immobilization process of probe, the conformational parameters (mass, thickness and density values) were analyzed out based on the TM and TE changes. When the positively charged PEI was injected into the bare silicon oxynitride chip surface, the mass and thickness increased quickly while the density decreased accordingly at the initial absorption period. Subsequently, the rate of absorption slowed down and tended to a stable value, which meant the absorption of PEI reached saturated state. When the negatively charged T30 was injected, the mass, thickness and density increased rapidly at the beginning, owing to the rapid absorption of T30. Then the mass and thickness slowly decreased at a similar rate while the density increased slightly, indicating that a more compact T30 layer formed. When the buffer solution re-injected into the T30 surface, the mass and thickness decreased indistinctively until reached a plateau, the density almost maintained a stable value. The reason was that some weakly absorbed T30 were washed away. After the injection of probe DNA, the mass and thickness were increased but the density of probe was decreased rapidly at first, and finally them reached a stable value. Real-time changes from mass, thickness and density parameters of probe illustrated that the probe had been successfully immobilized on the sensing surface.

On the basis of mass, thickness and density parameters displayed in Table 1, the surface conformation (distribution and state) of PEI, T30 and probe can be estimated. When PEI was introduced into both channels, a PEI layer with the thickness of 1.951 nm was formed. After the introduction of T30, the thickness of the layer increased by 1.02 nm, and the density

Table 1. Key parameters for probe/T30/PEI (Mean ± SD, n=3)

Layer material	Mass (ng/mm^2)	thickness (nm)	density (g/cm^3)
PEI	1.255 ± 0.192	1.951 ± 0.311	0.647 ± 0.0696
T30/PEI	2.219 ± 0.370[a]	2.971 ± 0.331[a]	0.745 ± 0.0632[a]
probe/T30/PEI	3.226 ± 0.472[a]	6.082 ± 0.515[a]	0.533 ± 0.0920[a]

[a] Mass, thickness, and density of the whole T30/PEI or probe/T30/PEI layer.

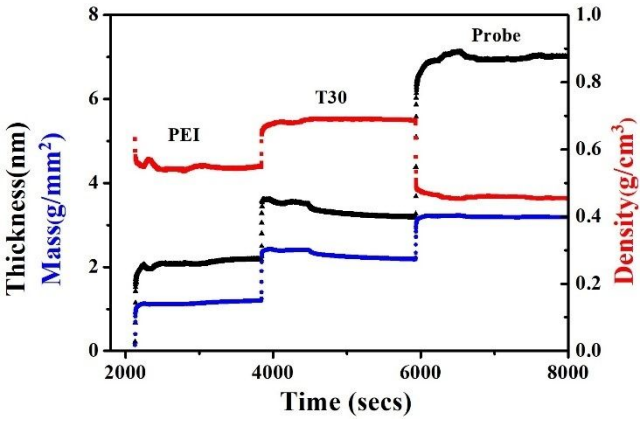

Figure 3. The mass (blue circle), thickness (black triangles) and density (red squares) for the whole immobilization process of PEI, T30 and probe on the bare silicon oxynitride by the real-time DPI measurements.

also increased. It has been illustrated that a DNA strand is about 1.90 nm wide[54] and each base in homothymine DNA oligonucleotide is approximately 0.52 nm in length[55], so the length of T30 was about 15.60 nm. The wide and length values of T30 layer were higher than thickness. Additionally, if the T30 had a "end-on" or "flat-on" conformation, the theoretical surface area value for per molecule was about 3.61 or 29.64 nm^2, respectively. However, the actual surface area value for per molecule calculated from the reported formula[33] was about 15.61 nm^2. These results indicated that, on the PEI surface, most T30 molecules might deposit predominantly as a flat monolayer and insert themselves partly into the PEI layer, making T30 attached on the surface tightly. After the immobilization of probe DNA, the thickness of the layer further increased by about 3 nm. This value lied in the range of 1.90 nm to 22.05 nm for horizontal orientation and vertical orientation of probe DNA, assuming that the average length of four bases is 0.63 nm in a ssDNA.[56] This result implied that the DNA probe may be oriented in an intermediate state between horizontal and vertical. Comparing with T30 layer, probe layer had a lower density but higher thickness, suggesting that the probe with little steric hindrance was highly water-swollen and almost unaffected by PEI.[57] So, the functional probe layer was more flexible to interact with Cd^{2+}.

Furthermore, to depict the whole conformational change process of the sensing platform construction, the changes in layer thickness and density of PEI, T30 and probe were also plotted as a function of respective mass loading. As shown in Figure 4,

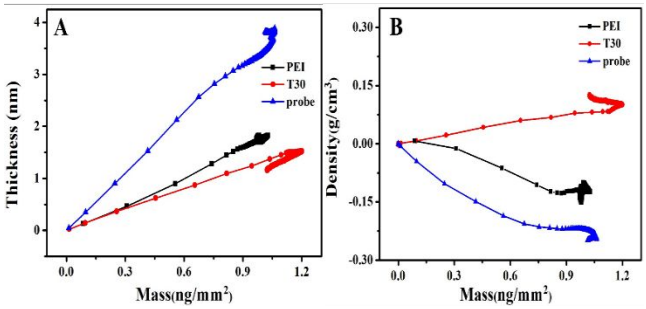

Figure 4. Changes in the layer thickness (A) and density (B) as functions of mass loading of PEI, T30 and probe during the entire construction process of aptasensor.

we could clearly observe the adsorption or response rate by analyzing the distribution of the data points which had the same collecting time intervals. At the beginning of injection, all data points were sparsely distribution, suggesting a fast absorption process. Then the dense point distribution indicated that the adsorption or response reached saturation and equilibrium. After that, with the injection of running buffer, the desorption or conformational rearrangement process of PEI, T30 and probe occurred.

Real-time monitor the interaction of aptamer with Cd^{2+} by DPI. After successfully establishing the sensing layer, the interaction between aptamer and Cd^{2+} on the solid- liquid interface can be studied. So as to understand the interaction process of probe and Cd^{2+} more clearly, the thickness and density of the probe layer as a function of mass loading were plotted with different concentrations of Cd^{2+}. Based on the experiment results (Figure S2), 0.36 mg/L Cd^{2+} was selected as a boundary concentration where the interaction phenomenon was divided into two trends. The typical curves of low Cd^{2+} concentration (0.018 mg/L) and high Cd^{2+} concentration (3.60 mg/L) are presented in Figure 5. When low concentration of Cd^{2+} was introduced, the thickness gradually increased and the density decreased with the increase of mass loading (Figure 5A and B). We speculated that Cd^{2+} mainly interacted with probe by binding to the phosphate group.[58] This interaction manner partially neutralized the negative charge of DNA sequence and reduced the repulsion between probe, which made DNA probe extend into the solution and enabled the random coil ssDNA structure to stretch.[59] After adding the high concentration of Cd^{2+} (Figure 5C and D), with the increase of mass loading, the thickness decreased while the density increased. This result indicated that Cd^{2+} primarily bound with bases via coordination interaction, promoting the π-π stack of bases and resulting in the conformation of probe transition from ssDNA or a few

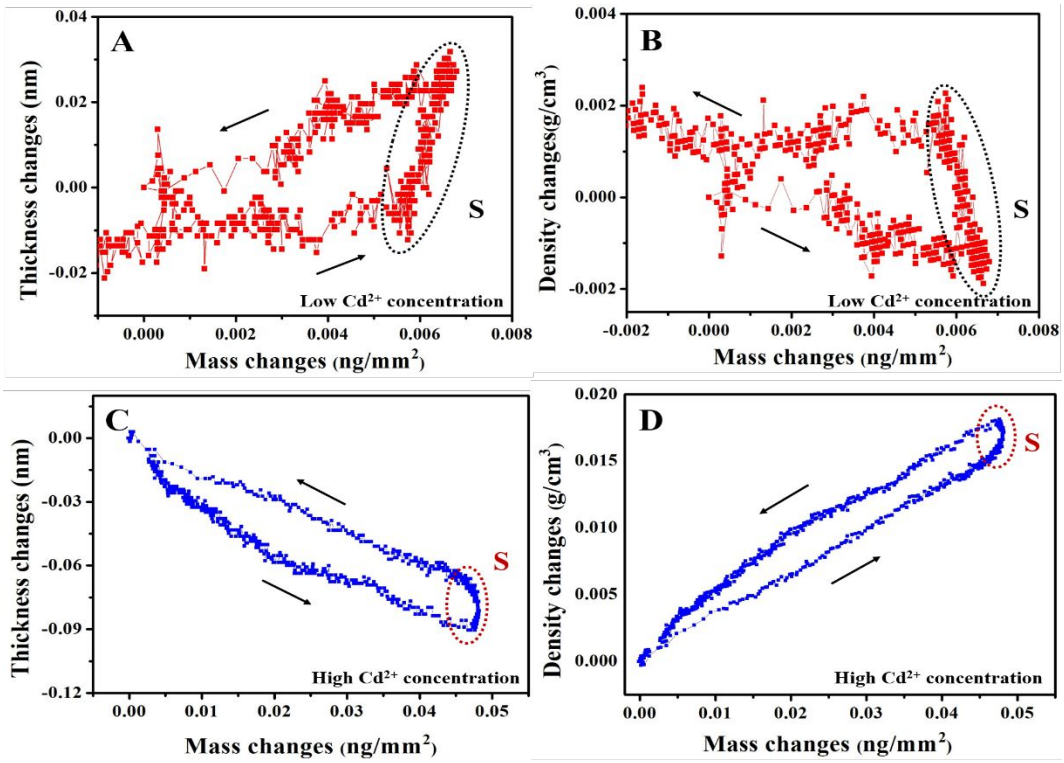

Figure 5. The whole dynamic process of interaction between Cd^{2+} and probe. Layer thickness (A, C) and density (B, D) of probe as a function of mass loading are researched under low (A, B) and high (C, D) Cd^{2+} concentration. Cd^{2+} concentration is 0.018 mg/L for low Cd^{2+} concentration and 3.60 mg/L for high Cd^{2+} concentration. Short arrows are presented the start and finish of interaction process. The black and wine-red loops S display the turning region.

hairpins to a tight and short hairpin structure. What's more, we analyzed the data points to further specify the dynamic of whole interaction process. Due to the data points were recorded with the same time intervals, so we could judge the binding rate according to the distribution of these points. We divided the whole interaction process into three parts through the turning region S (Figure 5). Before and behind the S region, the point was distributed densely, indicating that the binding process of probe and Cd^{2+} was slowly and tightly. In the S region, the point became more densely and the mass hardly changed. The trend of S region demonstrated that association rate and disassociation rate were gradually reached equilibrium. In a word, the interaction process of probe and Cd^{2+} mainly included three slow processes which were association, equilibrium and disassociation. In order to further illustrate the conformation change of DNA aptamer depending on the concentrations of Cd^{2+}, the two fluorescence experiments were carried out by using dsDNA specific fluorescence dye (SYBR Green I) and distance-dependent fluorescence resonance energy transfer (FRET), respectively (Figure S7, S8, and the discussion in Supporting Information). The results further verified the conformational change of aptamer after binding with Cd^{2+} ions.

Establishment of DPI-based Cd^{2+} aptasensor. For the sake of obtaining the kinetics and thermodynamics information of the Cd^{2+}/aptamer interaction, different Cd^{2+}concentration ranging from 0.0036 to 29.15 mg/L was introduced into the probe layer. Figure 6A shows that the mass increased with the increase of Cd^{2+} concentration. The density increased and the thickness decreased with the increase of Cd^{2+} concentration (Figure S3A and B). Eventually, these structure parameters can almost return to the original position via flowing the running buffer for ten minutes, suggesting that the biosensing platform can be regenerated (Figure S4). From changes of the real-time binding curve of mass, the association rate constant (k_a), dissociation rate constant (k_d) and disassociation constant (K_D) between Cd^{2+} and its aptamer were calculated to be 96 $M^{-1}\bullet S^{-1}$, 2.11 $\times$ 10^{-5} S^{-1}, and 220 nM, respectively, the disassociation constant (K_D) is approximated to other studies.[18] Moreover, as displayed in Figure 6B, the change of mass values was proportional to the concentrations of Cd^{2+} ranging from 0.0036 to 18.22 mg/L, and the changes of thickness and density values were exhibited in Figure S3C and D. At the high Cd^{2+} concentration exceeding 7.28 mg/L, the structure parameters showed different trends, this may be attributed to either a more complex binding process or the already saturated binding sites. Based on above experiments phenomena, a DPI-based Cd^{2+} was established through layer-by-layer assembly method. The mass (the insert in Figure 6B), density and thickness (inserts in Figure S3C and D) were linearly related to the concentration of Cd^{2+} in the range from 0.0036 to 7.28 mg/L. The linear calibration equation was Mass (ng/mm²) = 0.00145c + 0.01161 (R^2 = 0.998), where Cd^{2+} concentration c had units of milligram per liter. The limit of detection (3σ) were 0.61 μg/L for mass calibration. This value was lower than a lowest limit concentration (5.0 μg/L) recommended by US Environmental Protection Agency (EPA) for Cd (II) in drinking water. Hence, this aptasensor can be used to quantify the Cd^{2+} in real samples.

Specificity and selectivity of Cd^{2+}-aptamer binding. A control ssDNA, having a random sequence and same length with probe, was utilized to assess the specificity of Cd^{2+} binding to aptamer. As can be seen from Figure S5, after adding different

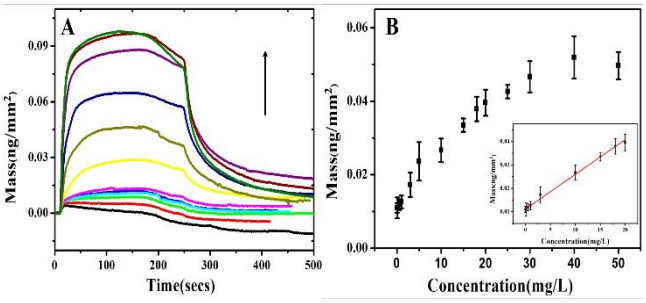

Figure 6. The real-time mass change trends (A) and linearity range (B) of probe layer with adding different concentrations of Cd^{2+}. The arrow in (A) shows increasing Cd^{2+} concentration from 0.0036 to 29.15 mg/L, the Cd^{2+} concentration of plot (B) ranges from 0.0036 to 18.22 mg/L. The arrow bars present the standard deviation of three measurements. The inset shows expanded linear region.

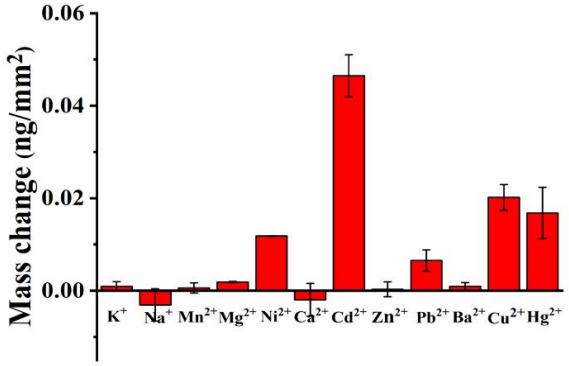

Figure 7. Selectivity of Cd^{2+} aptasensor. Histograms present mass changes. The concentration of all metal ions is 7.28 mg/L.

concentrations of Cd^{2+}, the probe layer had obvious changes in mass, thickness and density, while the control DNA layer had negligible changes, illustrating the highly specific binding of Cd^{2+} towards aptamer.

The selectivity of the developed aptasensor for Cd^{2+} against other metal ions, such as K^+, Na^+, Mn^{2+}, Mg^{2+}, Ni^{2+}, Ca^{2+}, Zn^{2+}, Pb^{2+} and Ba^{2+}, were also investigated. As displayed in Figure 7 and Figure S6, the aptasensor shows small or negligible response to these interfering ions compared with Cd^{2+}, suggesting that the aptasensor also has good selectivity for Cd^{2+}. For Hg^{2+} and Cu^{2+} ions, however, the responses are higher than other investigated metal ions (except for Cd^{2+}). Therefore, it is necessary to adopt an appropriate method to eliminate the interference, for example, introducing chelating reagent 2,6-pyridinedicarboxylic acid (PDCA),[60] or adjusting the solution pH.[17]

Detection of Cd^{2+} in real sample. The practical performance of aptasensor also evaluated by means of monitoring Cd^{2+} in tapping water as a real sample. Cd^{2+} with different concentrations were spiked into the 1% real sample diluted with the buffer solution and tested by DPI technique. Figure S9 exhibited the real-time measurement curves for adding different concentrations of Cd^{2+} in real samples. Three groups of concentration data were acquired based on the mass, thickness and density calibrations, and the results were summarized in Table S2. The recoveries were ranging from 99% to 133% with the RSDs from 0.26 to 13.93. So, this aptasensor has the potential to analyze Cd^{2+} in real samples.

CONCLUSION

In summary, on the basis of the specific binding of Cd^{2+} with aptamer and the real-time, lable-free DPI technique, a DPI-based Cd^{2+} aptasensor was developed, which not only can quantify Cd^{2+} with high sensitivity and selectivity, but also can provide both kinetics and structural information during the whole interaction process. Combined with other spectroscopy characterization (FTIR, CD, UV-vis), the principle of interaction between Cd^{2+} and aptamer was clarified. Compared with previous detection methods, the aptasensor has some advantages such as low cost, regeneration and obtaining the kinetic constant. What's more, the DPI-based Cd^{2+} aptasensor has two detection channels, realizing the multi-channel simultaneous detection function at one time. Therefore, more aptamer-based biosensor can be constructed by DPI technique to realize the detection of other ions, small molecules, or biomacromolecules and explore the interaction of DNA with them simultaneously.

ASSOCIATED CONTENT

Supporting Information

The Supporting Information is available free of charge on the ACS Publications website.

All of the sequences used in experiment (Table S1), the melting cure of probe with or without Cd^{2+} (Figure S1), whole dynamic process of interaction between Cd^{2+} and probe (Figure S2), thickness and density change trends and linearity range of Cd^{2+} aptasensor (Figure S3), the regeneration plot of Cd^{2+} aptasensor (Figure S4), specificity and selectivity of Cd^{2+} aptasensor (Figure S5 and S6), fluorescence experiments of probe with Cd^{2+} (Figure S7 and S8), detection of Cd^{2+} in real samples (Figure S9 and Table S2).

AUTHOR INFORMATION

Corresponding Author

* E-mail: xryang@ciac.ac.cn. Phone: +86 431 85262056. Fax: +86 431 85689278.
* E-mail: huangjs@ciac.ac.cn Phone: +86 431 85262964. Fax: +86 431 85689278.

Notes

The authors declare no competing financial interest.

ACKNOWLEDGMENTS

This work was supported by the National Natural Science Foundation of China (No. 21627808 and 21721003), the Key Research Program of Frontier Sciences, CAS (QYZDY-SSW-SLH019).

REFERENCES

(1) Hutton, M. *Ecotoxicol. Environ. Saf.* **1983**, 7, 9–24.
(2) Song, T.; Zhu, X. F.; Zhou, S. H.; Yang, G.; Gan, W.; Yuan, Q. H. *Appl. Surf. Sci.* **2015**, 347, 505-513.
(3) Hua, Z. L.; Yang, B.; Chen, W.; Bai, X.; Xu, Q. J.; Gu, H. X. *Appl. Surf. Sci.* **2014**, 317, 226-235.
(4) Kim, H. N.; Ren, W. X.; Kim, J. S.; Yoon, J. *Chem. Soc. Rev.* **2012**, 41, 3210-3244.
(5) Flick, D. F.; Kraybill, H. F.; Dlmitroff, J. M. *Environ. Res.* **1971**, 4, 71-85.
(6) U. S. E. P. Agency, in National Primary Drinking Water Regulations, 2009, http://water.epa.gov/drink/contaminants/.
(7) Ellington, A. D.; Szostak, J. W. *Nature* **1990**, 346, 818-822.
(8) Tuerk, C.; Gold, L. *Science* **1990**, 249, 505-510.

(9) Zhou, W. H.; Ding, J. S.; Liu, J. W. *Biosens. Bioelectron.* **2017**, 87, 171–177.
(10) Guo, Y. Q.; Chen, Y. X.; Wei, Y.; Li, H. H.; Dong, C. *Spectrochim. Acta, Part A: Mol. and Biomol. Spectrosc.* **2015**, 136, 1635–1641.
(11) Shamsipur, M.; Farzin, L.; Tabrizi, M. A.; Shanehsaz, M. *Mater. Sci. Eng. C* **2016**, 69, 1354–1360.
(12) Zhang, S. B.; Wang, L. P.; Liu, M. L.; Qiu, Y. Q.; Wang, M. N.; Liu, X. W.; Shen，G. L.; Yu, R. Q. *Anal. Methods* **2016**, 8, 3740–3746.
(13) Tabrizi, M. A.; Shamsipur, M.; Farzin, L. *Biosens. Bioelectron.* **2015**, 74, 764–769.
(14) Shamsipur, M.; Farzin, L.; Tabrizi, M. A. *Microchim. Acta* **2016**, 183, 2733–2743.
(15) Farzin, L.; Shamsipur, M.; Sheibani, S. *Talanta* **2017**, 174, 619-627.
(16) Zhou, B.; Wang, Y. S.; Yang, H. X.; Xue, J. H.; Wang, J. C.; Liu, S. D.; Liu, H.; Zhao, H. *Microchim. Acta* **2014**, 181, 1353–1360.
(17) Wang, H. Y.; Cheng, H.; Wang, J. N.; Xu, L. J.; Chen, H. X.; Pei, R. J. *Talanta* **2016**, 154, 498–503.
(18) Wu, Y. G.; Zhan, S. S.; Wang, L. M.; Zhou, P. *Analyst* **2014**, 139, 1550-1561.
(19) Luan, Y. X.; Lu, A. X.; Chen, J. Y.; Fu, H. L.; Xu, L. *Appl. Sci.* **2016**, 6, 432-436.
(20) Zhou, B.; Yang, X. Y.; Wang, Y. S.; Yi, J. C.; Zeng, Z.; Zhang, H.; Chen, Y. T.; Hu, X. J.; Suo, Q. L. *Microchem. J.* **2019**, 144, 377–382.
(21) Zhu, Y. F.; Wang, Y. S.; Zhou, B.; Yu, J. H.; Peng, L. L.; Huang, Y. Q.; Li, X. J.; Li, S. H.; Tang, X.; Wang, X. F. *Anal. Bioanal. Chem.* **2017**, 409, 4951-4958.
(22) Lotfi Zadeh Zhad, H. R.; Rodríguez, Y. M.; Lai, R. Y. J. *Electroanal. Chem.* **2017**, 803, 89–94.
(23) López-García, I.; Vicente-Martínez, Y.; Hernández-Córdoba, M. *Talanta* **2013**, 110, 46-52.
(24) Krawczyk, M.; Skowron, M. J. *Microchem. J.* **2015**, 126, 296-301.
(25) Yu, X. X.; Chen, B. B.; He, M.; Wang, H.; Hu, B. *Talanta* **2018**, 179, 279-284.
(26) Kim, H. N.; Ren, W. X.; Kim, J. S.; Yoon, J. *Chem. Soc. Rev.* **2012**, 41, 3210–3244.
(27) Escorihuela, J.; González-Martínez, M. Á.; López-Paz, J. L.; Puchades, R.; Maquieira, Á.; Gimenez-Romero, D. *Chem. Rev.* **2015**, 115, 265–294.
(28) Schneider, B. H.; Edwards, J. G.; Hartman, N. F. *Clin. Chem.* **1997**, 43, 1757-1763.
(29) Freeman, N. In Proteins. Solid-Liquid. Interfaces; Dejardin, P., Ed.; Springer: Berlin, Heidelberg, **2006**, pp 75-104.
(30) Wan, Y. B.; Li, X. H. Chin. J. *Anal. Chem.* **2015**, 43, 1203-1209.
(31) Huang, G. L.; Yuan, L.; Liu, S. L.; Zhou, S. K. Chin. J. *Anal. Chem.* **2015**, 43, 1927-1933.
(32) Hu, T.; Wang, S.; Chen, C. X.; Sun, J.; Yang, X. R. *Anal. Chem.* **2017**, 89, 2606-2612.
(33) Wang, Y.; Wang, J.; Yang, F.; Yang, X. R. *Anal. Chem.* **2012**, 84, 924-930.
(34) Wang, J.; Xu, X. W.; Zhang, Z. X.; Yang, F.; Yang, X. R. *Anal. Chem.* **2009**, 81, 4914-4921.
(35) Wang, Y.; Zheng, Y.; Yang, F.; Yang, X. R. *Chem. Commun.* **2012**, 48, 2873-2875.
(36) Zheng, Y.; Yang, C.; Yang, F.; Yang, X. R. *Anal. Chem.* **2014**, 86, 3849-3855.
(37) Wang, S.; Lu, S. S.; Zhao, J. H.; Huang, J. S.; Yang, X. R. *ACS Appl. Mater. Interfaces* **2017**, 9, 41568-41576.
(38) Lee, T. H.; Heng, C.; Separovic, F.; Aguilar, M. I. *Biochim. Biophys. Acta, Biomembr.* **2014**, 1838, 2205-2215.
(39) Lee, T. H.; Heng, C.; Swann, M. J.; Gehman, J. D.; Separovic, F.; Aguilar, M. I. *Biochim. Biophys. Acta, Biomembr.* **2010**, 1798, 1977-1986.
(40) Bijelic, G.; Shovsky, A.; Varga, I.; Makuska, R.; Claesson, P. M. *J. Colloid Interface Sci.* **2010**, 348, 189-197.
(41) Jin, J.; Huang, F. J.; Hu, Y.; Jiang, W.; Ji, X. L.; Liang, H. J.; Yin, J. H. *Colloids Surf., B* **2014**, 123, 892-899.
(42) Wang, S.; Lu, S. S.; Zhao, J. H.; Huang, J. S.; Yang, X. R. *Talanta* **2019**, 202, 336-341.
(43) Alex, S.; Dupuis, P. *Inorg. Chim. Acta* **1989**, 157, 271-281.
(44) Jangir, D. K.; Tyagi, G.; Mehrotra, R.; Kundu, S. *J. Mol. Struct.* **2010**, 969, 126-129.
(45) Tajmir-Riahi, H. A.; Theophanides, T. *Can. J. Chem.* **1983**, 61, 1813-1822.
(46) Tsuboi, M. *Appl. Spectr. Rev.* **1969**, 3, 45-74.
(47) Taillandier, E.; Ridoux, J. P.; Liquier, J.; Leupin, W.; Denny, W. A.; Wang, Y.; Thomas, G. A.; Peticolas, W. L. *Biochemistry* **1987**, 26, 3361-3368.
(48) Tsuboi, M.; Takahashi, S.; Harada, I. *Phys.-Chem. Prop. Nucleic Acids* **1973**, 2, 91-143.
(49) Keller, P. B.; Hartman, K. A. *Spectrochim. Acta, Part A* **1986**, 42, 299-306.
(50) Shimanouchi, T.; Tsuboi, M.; Kyogoku, Y. *Adv. Chem. Phys.* **1964**, 7, 435.
(51) Zheng, B.; Cheng, S.; Liu, W.; Lam, M. H-W.; Liang, H. J. *Anal. Chim. Acta* **2012**, 741, 106–113.
(52) Jangir, D. K.; Dey, S. K.; Kundu, S.; Mehrotra, R. J. *Photochem. Photobiol., B* **2012**, 114, 38-43.
(53) Lee, J. H.; Wang, Z. D.; Liu, J. W.; Lu, Y. *J. Am. Chem. Soc.* **2008**, 130, 14217-14226.
(54) Johnston, A. P. R.; Read, E. S.; Caruso, F. *Nano Lett.* **2005**, 5, 953-956.
(55) Mills, J. B.; Vacano, E.; Hagerman, P. J. *J. Mol. Biol.* **1999**, 285, 245-257.
(56) Murphy, M. C.; Rasnik, I.; Cheng, W.; Lohman, T. M.; Ha, T. *Biophys. J.* **2004**, 86, 2530-2537.
(57) Lee, L.; Johnston, A. P. R.; Caruso, F. *Biomacromolecules* **2008**, 9, 3070-3078.
(58) Eichhorn, G. L.; Shin, Y. A. *J. Am. Chem. Soc.* **1968**, 90, 7323-7328.
(59) Huang, F. J.; Xu, P. P.; Liang, H. J. *Biosens. Bioelectron.* **2014**, 51, 317-323.
(60) Li, D.; Wieckowska, A.; Willner, I. *Angew. Chem. Int. Ed.* **2008**, 47, 3927–3931.

For TOC only